

Effect of Partial Substitution of Nickel by Tin, Aluminum, Manganese and Palladium on the Properties of LaNi_5 -Type Metal Hydride Alloys

Elki C. Souza and Edson A. Ticianelli*

Instituto de Química de São Carlos, Universidade de São Paulo, CP 780, 13560-970 São Carlos - SP, Brazil

Neste trabalho é feito um estudo do comportamento eletroquímico de eletrodos formados por pó de ligas de hidreto metálico do tipo AB_5 com formulações $\text{LaNi}_{(5-x)}\text{Z}_x$, onde Z é um elemento metálico que substitui parcialmente o Ni, que inclui Sn, Al, Mn e Pd. No caso do Mn, algumas estruturas do tipo AB_6 são também consideradas. A substituição de uma pequena fração do Ni pelo Al, Sn e Mn ($x \cong 0.3$) promove um aumento da capacidade de armazenamento de hidrogênio (CAH), enquanto que o Pd leva à um decréscimo desta propriedade. Em geral todas as ligas apresentam alta CAH inicial, mas exibem baixa estabilidade. Foi observado que a diminuição da pressão de equilíbrio de hidrogênio em função do teor de Mn, nas ligas AB_5 , relaciona-se diretamente com o aumento do volume da cela cristalina unitária. Através de experimentos de impedância eletroquímica nota-se um aumento significativo da cinética de reação de hidratação/desidratação com o aumento do número de ciclos de carga/descarga do eletrodo, devido ao aumento da área ativa. Também foi observado que, no geral, as ligas que apresentam maior CAH são aquelas que possuem menor energia de ativação para a reação de oxidação de hidrogênio.

This work reports studies on the electrochemical behavior of AB_5 -type hydrogen storage alloys, formed by $\text{LaNi}_{(5-x)}\text{Z}_x$, where Z is a metallic element partially replacing Ni, which included Sn, Al, Mn, and Pd. In the case of Mn, some AB_6 -type structures were also considered. Substitution of a small fraction of Ni by Al, Sn, and Mn ($x \cong 0.3$) leads to an increase of the hydrogen storage capability (HSC), while for Pd there is a decrease of this property. Generally all alloys presenting larger initial HSC exhibit lower stability. A decrease of the hydrogen equilibrium pressure as a function of Mn content is observed for the AB_5 alloys and this is related to an increase of the crystalline unit cell volume. Electrochemical impedance measurements show a significant increase of the hydration/dehydration reaction kinetics due to a raise on the active area as a function of the charge/discharge cycle number. It is also seen that the alloys presenting larger HSC are those showing smaller activation energies for the hydrogen oxidation reaction.

Keywords: hydrogen storage materials, electrode materials, energy storage materials, nickel-metal hydride battery

Introduction

The use of metal-hydride (MH) alloys as negative electrode material in rechargeable alkaline batteries has grown in recent years, because of its high energy density, high rate capability, and environmental acceptability. Ni-MH batteries have been developed and commercialized to meet a strong market demand as a power source with a high performance/cost ratio.^{1,2} Currently, the anodes of most Ni-MH batteries are based on the AB_5 family of intermetallic compounds. To improve the electrode performance and lower costs of hydrogen storage alloys, AB_5 type alloys

have been developed with substitution of pure earth elements in A side (La) by a mischmetal-based multi-component and the partial replacement of Ni in B side by Co, Mn, Al, *etc.* The effects of the replacement on both A and B sides on the performances, the discharge capacity, cycle life, *etc.*, of the alloy electrodes have been extensively investigated by many researchers.²⁻¹¹

The partial substitution of Ni by Co in many alloys increases the thermodynamic stability of the hydride phase as well as its corrosion resistance, providing a long cycle life.^{12,13} The effects have been attributed to a diminution in the volume changes upon hydrogen absorption and desorption and to a surface passivation mechanism (*i.e.*, oxide formation) and a smaller stress-cracking

* e-mail: edsont@iqsc.usp.br

phenomenon due to a lowering of the Vickers hardness.¹⁴ However, Co is responsible for a large fraction of the total raw material cost.

Investigations have been also done using Sn or Al as a partial substituent for Ni in LaNi_5 .^{6,8,15-18} The substitution of small amounts of Sn or Al improves many characteristics of the metal hydride anode with the increase of the unit cell volume and the reduction of absorption plateau pressure. In fact, several other metals turned out to be good candidates in lowering the plateau pressure.^{2,9,19-21} Nowadays, Mn is widely applied in commercial stoichiometric hydride-forming compounds. According to Notten *et al.*,⁹ compounds with nominal composition $\text{La}(\text{Ni}_{1-z}\text{Mn}_z)_x$, in which the stoichiometry was varied in the range $5.0 \leq x \leq 6.0$ have practically the same initial charge storage capacity. Results show that the oxidation rate is strongly dependent on both the chemical composition of the hydride-forming compound, in this case on the Mn content (z), and the degree of non-stoichiometry (x), suggesting that the electrochemical cycling stability can be further improved by fine-tuning both these parameters.^{9,21} In more complex alloys, the function of Mn is still an open question.²¹ Generally for many alloys, the electrochemical behavior depends on the structure, the nature and amount of each element in the intermetallic compound, and the electrochemical process(es) taking place in the particle surface.

In this work a comparative study of the effects of Ni substitution by Sn, Al, Pd, and Mn atoms on the charge storage capacity, the cycling life, the hydrogen equilibrium pressure, and the charge-discharge reaction kinetics in AB_5 -type compounds is carried out. In the case of Mn, some AB_6 -type structures were also considered. In all cases the lattice parameters of the alloy unit cell were obtained by X-ray diffraction analyses. Experimental results were analyzed taking into account the thermodynamic and the electronic effects introduced by the replacing element to the alloy, an approach which has not been considered before.

Experimental

The alloys were prepared from high-purity elements (99.9%), melted in an arc furnace under an argon atmosphere (analytic 5.0, White Martins). The samples were turned over and remelted several times. To ensure homogeneous distribution of the elements in the alloys, the ingots were subsequently annealed in vacuum at 950 °C for 72 h. Next, the ingots were mechanically pulverized until obtaining particle sizes around 30 μm . Energy Dispersive X-ray analyses (100 times magnifi-

cation) made at several spots were used to obtain the real composition of the alloys. X-ray diffraction (XRD) analyses were made in order to verify the crystalline structure of the prepared alloys and these experiments were conducted using a URD6 – Zeiss Zena model universal X-ray diffractometer with $\text{Cu K}\alpha$ ($\lambda = 1.54 \text{ \AA}$).

Electrodes were prepared by pressing a mix comprised of 0.05 g of the alloy powder, 0.05 g of carbon black (Vulcan XC-72R) containing 33 weight percent (wt%) polytetrafluorethylene (PTFE, Teflon T-30, E. I. DuPont) on both sides of a nickel-screen with a geometric area of 2.0 cm^2 . All electrochemical measurements were made in a three-electrode system, consisting of a negative electrode, a counter electrode and an Hg/HgO reference electrode. The electrolyte was KOH 6.0 mol L^{-1} .

In the charge-discharge cycle tests, the negative electrode was charged at 10 mA for 2 h and discharged at the same current down to a cutoff potential of -0.7V vs. Hg/HgO KOH 6.0 mol L^{-1} . Electrochemical impedance spectra (EIS) were obtained using an Autolab (model PGSTAT 30) electrochemical impedance analyzer. The ac amplitude was 5 mV, which satisfies the linear polarization requirements, and the frequency range was from 1 mHz to 10 kHz. The impedance measurements were conducted at different temperatures, in order to access the activation energy of the hydrogen oxidation reaction (HOR).

For measurements of the hydrogen equilibrium pressure as a function of the state of charge, the activated electrode was fully charged and maintained at open-circuit until the potential reached equilibrium (variation of less than 0.1 mV min^{-1}). Then, the electrodes were partially discharged and the equilibrium potential measured again. This procedure was repeated until the electrode was fully discharged. The partial hydrogen pressures were calculated from the equilibrium potential (E_{MH}^{eq}) using the Nernst equation.^{9,22}

Results and Discussion

Diffraction data were obtained for all alloys investigated. Figure 1 shows the X-ray diffraction (XRD) pattern for AB_5 and AB_6 alloy powders with different Mn contents. The numbers on the main peaks correspond to the Miller (hkl) planes and the inset corresponds to the enlargement of the diffraction signal in the range $29 < 2\theta < 32$, for the (101) Miller indices.

These results show that the alloys present hexagonal CaCu_5 -type structure, in agreement with Vogt *et al.*⁸ No extra peak was observed for all alloys evidencing negligible phase segregation. The diffraction peaks shifted to smaller angles (as illustrated in the inset), implying an

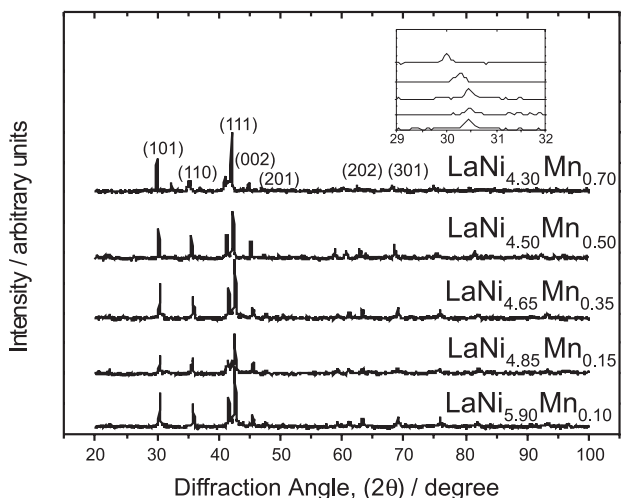


Figure 1. X-ray diffraction patterns for $\text{LaNi}_{5-x}\text{Mn}_x$ and $\text{LaNi}_{6-x}\text{Mn}_x$ alloys. The numbers on the main peaks correspond to the Miller (hkl) planes and the inset corresponds to the enlargement of the diffraction signal in the range $29 < 2\theta < 32$, for the (101) Miller indices.

Table 1. Lattice parameters obtained from XRD measurements

Alloy	a (Å)	c (Å)	V (Å ³)
LaNi_5	5.01395	3.98221	86.7
$\text{LaNi}_{4.7}\text{Sn}_{0.3}$	5.05339	4.02234	89.0
$\text{LaNi}_{4.7}\text{Pd}_{0.3}$	5.04216	3.99268	87.9
$\text{LaNi}_{4.7}\text{Al}_{0.3}$	5.02447	4.00372	87.5
$\text{LaNi}_{4.85}\text{Mn}_{0.15}$	5.01319	3.97531	86.5
$\text{LaNi}_{4.65}\text{Mn}_{0.35}$	5.04774	4.00748	88.4
$\text{LaNi}_{4.30}\text{Mn}_{0.70}$	5.07480	4.04072	90.1
$\text{LaNi}_{5.90}\text{Mn}_{0.10}$	5.04216	3.99268	86.4
$\text{LaNi}_{5.50}\text{Mn}_{0.50}$	5.04158	4.00606	88.2

increase in the lattice parameters with partial replacement of Ni by Mn, Sn, Al and Pd in the AB_5 alloys. Table 1 presents the values of the crystallographic axes and the unit cell volumes obtained from the XRD data.⁹

From the results in Table 1 it is seen that substitution of a small fraction of Ni ($x \sim 0.3$) by Sn and Pd leads to an increase of the crystallographic parameters, following a good correlation with the values of the atomic radius, which increases in the order Ni (1.25 Å) < Pd (1.38 Å) < Sn (1.41 Å).²³ This trend is not confirmed in the case of Al (1.43 Å), as also observed in the literature,²¹ probably because specific electronic effects may determine the cell volume characteristics. As expected, in the case of stoichiometric (AB_5) and nonstoichiometric (AB_6) alloys with small Mn contents, no significant difference of the cell volume is observed compared to LaNi_5 . However, an increase of the cell volume with increasing Mn content is denoted by the XRD data for the AB_5 alloys, in agreement with the fact

that the atomic radius of Mn (1.26 or 1.30 Å, depending on the coordination number)⁹ is slightly higher than that of Ni. This is not the case for the Mn containing AB_6 alloy, in which case some of the excess amount of B-type atoms may be accommodated in the lattice position of La.⁹

The charge storage capacity and the alloy stability were measured from discharge capacity vs. cycle number profiles, as illustrated in Figure 2 for LaNi_5 , $\text{LaNi}_{4.7}\text{Sn}_{0.3}$, $\text{LaNi}_{4.7}\text{Al}_{0.3}$, $\text{LaNi}_{4.7}\text{Pd}_{0.3}$, and in the Figure 3 for electrodes formed by Mn containing alloys. The rates of the charge capacity decay were calculated from the slope of the discharge capacity plots in Figures 2 and 3, in the range between 20 to 40 cycles, where the profiles are essentially linear. Results are listed in Table 2, together with the maximum charge storage capacity attained for each alloy.

Results in Figure 2 show that the charge storage capacity of the LaNi_5 alloy resulted 125 mAh g⁻¹ in the first cycle, but it decreases exponentially to about 50 mAh g⁻¹ after

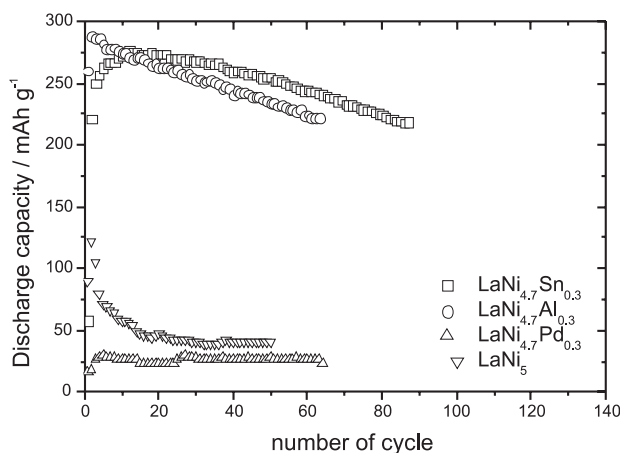


Figure 2. Discharge capacity as a function of the cycle number for the electrodes formed by AB_5 alloys.

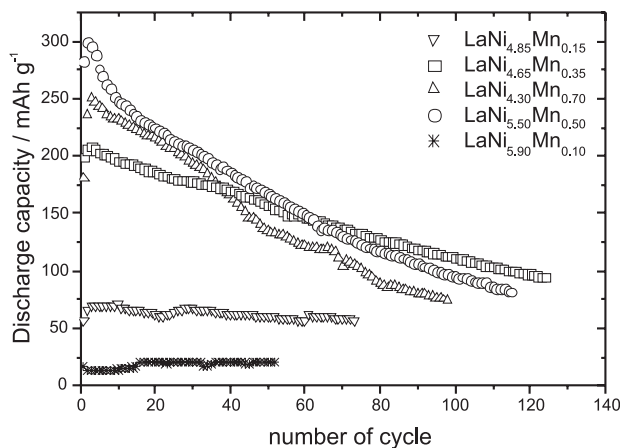


Figure 3. Discharge capacity as a function of the cycle number for the electrodes formed by Mn containing alloys.

Table 2. Maximum discharge capacity and the decay rate

Alloy type	Alloy	Maximum discharge capacity, mAh g ⁻¹	(-dQ/dcycle) mAh g ⁻¹ cycle ⁻¹
AB ₅	LaNi ₅	125	-
	LaNi _{4.7} Sn _{0.3}	276	0.66
	LaNi _{4.7} Al _{0.3}	290	0.99
	LaNi _{4.7} Pd _{0.3}	56	0.23
	LaNi _{4.85} Mn _{0.15}	70	0.13
	LaNi _{4.65} Mn _{0.35}	208	0.91
	LaNi _{4.30} Mn _{0.70}	250	1.84
AB ₆	LaNi _{5.90} Mn _{0.10}	22	0.02
	LaNi _{5.50} Mn _{0.50}	299	1.52

20 cycles. The initial charge storage capacity is much smaller than the theoretical value for LaNi₅H₆ (360 mAh g⁻¹) and this has been attributed to the corrosion of the alloy in contact with the alkaline electrolyte.¹²⁻¹⁴ The substitution of a small fraction of Ni by Al, Sn, and Mn ($x \geq 0.3$) leads to an increase of the maximum hydrogen storage capacity (HSC) measured in the electrochemical environment, and on the material stability as a function of the charge/discharge cycle number. Only in the cases of Pd ($x = 0.3$) and Mn ($x \sim 0.1$), a decrease of the maximum HSC is observed, compared to LaNi₅. However in these cases the values of HSC remain essentially constant as a function of the cycle number. For LaNi_{4.7}Al_{0.3} and LaNi_{4.7}Sn_{0.3}, the results are in good agreement with those reported previously.^{2,10,21,24}

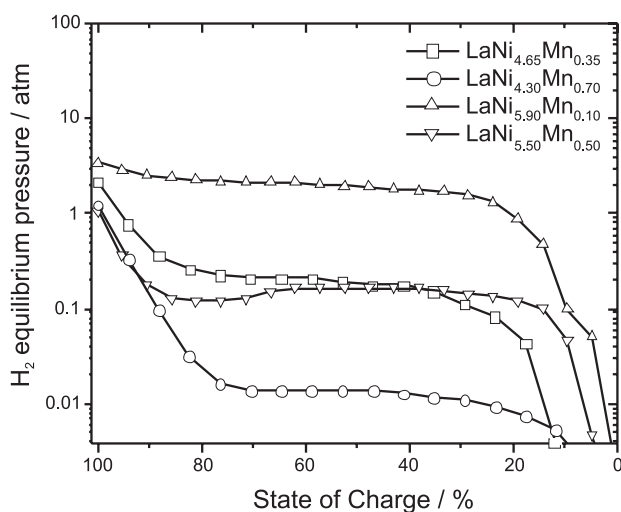
It has been observed that a more vacant Ni 3d electronic band leads to an increase of the HSC in AB₅-type metal hydride alloys.²⁵ Therefore, the differences on the maximum HSC among the different alloys could be attributed in principle to the different effects of the substituents on the 3d Ni band occupancy. In parallel to these electronic effects, an increase of the unit cell volume may also lead to an increase of the hydrogen storage capacity due to a decrease of the hydrogen chemical potential in the hydride phase.²⁶ In the present investigation, no general correlations can be established between the maximum HSC and the unit cell volumes for the different elements replacing Ni, indicating that the electronic effects of the substituents on the Ni band occupancy may be a primary effect determining the magnitude of the HSC is particularly. For the same metal substituent such as the Mn containing materials, a clear raise of the maximum HSC as a function of the Mn content is seen for the stoichiometric compounds, a fact which coincides with the raise of the cell volume and the reduction of the chemical potential of hydrogen.

The rate of the capacity decay of the MH electrode is

determined by the corrosion rate of the metal hydride alloy,^{6,27} which in turn is governed by two factors: the surface passivation due to the presence of surface oxides or hydroxides and the magnitude of molar volume of hydrogen inside the hydride phase. This last factor determines the expansion/contraction of the alloy unit cell during the charge-discharge cycles, eventually resulting in a stress-cracking of the particles. This causes pulverization of the MH alloy particles, raising the surface oxidation processes.

In Table 2 it is seen that in general the rates of capacity decay increase with the increase of HSC. This is consistent with the fact that a larger insertion of H in the unit cell leads to higher volume expansion and to a raise of the stress-cracking and the corrosion rates. These results show that there is no evident effect of the nature of the Ni substituent related to the surface passivation mechanism on the alloy stability. Thus, no specific effect of elemental chemical stability of the alloy components to the electrochemical environment, as for example proposed for Mn and Al containing materials,²⁸ can be detected. The important effects of the different elements on the alloy stability seem to be just those caused by the stress-cracking phenomenon associated to the changes on the molar volume of hydrogen.

Plots of the equilibrium pressure as a function of the state of charge for the metal hydride alloys based in the Mn composition are shown in Figure 4. As for many metal hydride alloys, a decrease of hydrogen equilibrium pressure with the reduction of the state of charge of the electrode is clearly observed. On the other hand, a correlation can be seen between the plateau pressure and the unit cell volume. To better illustrate this correlation, Figure 5 presents a

**Figure 4.** Hydrogen equilibrium pressure as a function of the state of charge, for the electrodes with different Mn contents.

plot of the plateau pressure as a function of the unit cell volume for the Mn containing alloys. Higher volumes of unit cell leads to smaller compression or chemical potential of the hydrogen atoms inside the crystal, diminishing the tendency of hydrogen to escape from the alloy. The very high equilibrium pressure for the $\text{LaNi}_{5.90}\text{Mn}_{0.10}$ resulted from the small unit cell volume presented by this alloy. This high equilibrium pressure can explain the low value of the HSC obtained for this electrode, because in this condition the hydride oxidation must occur in parallel with a fast release of absorbed hydrogen to the gas phase. For the other Mn contents the equilibrium pressures are at least one order of magnitude smaller compared to this alloy, indicating smaller gas release.

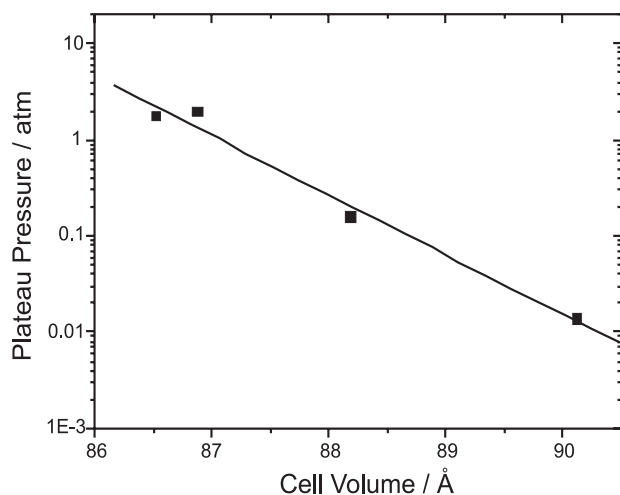
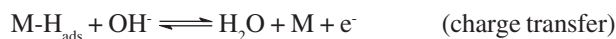
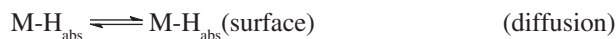


Figure 5. Change of the plateau pressure at 299 K as a function of the cell volume for $\text{LaNi}_{5-x}\text{Mn}_x$ and $\text{LaNi}_{6-x}\text{Mn}_x$ alloys.

Figure 6 presents Nyquist impedance plots for activated $\text{LaNi}_{5.50}\text{Mn}_{0.50}$ alloy electrodes in several of states charge at 26 °C (Fig. 6a), and for $\text{LaNi}_{4.30}\text{Mn}_{0.70}$ alloy electrodes at several temperatures (Figure 6b). Results show the presence of a high-frequency arc (10 kHz to 10 Hz), as illustrated in the inset in Figure 6b. This feature is related to the presence of a contact resistance between the current collector and the active material.^{12,26,27,29-32} Previous works have shown that the kinetics of the hydriding-dehydriding processes, may be governed either by a diffusion or a charge transfer steps:



The arc in the range of 200 Hz to 10 mHz has been associated to the charge-transfer resistance of the HOR at the electrode/electrolyte interface, as observed for most

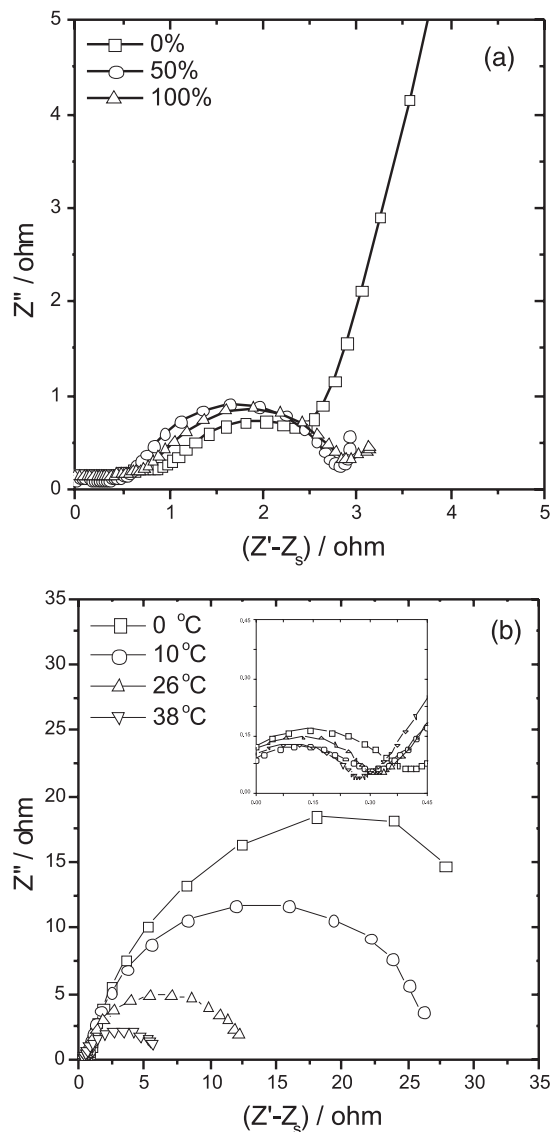


Figure 6. Nyquist plots for the metal hydride electrodes: (a) effect of the state of charge for the $\text{LaNi}_{5.50}\text{Mn}_{0.50}$ alloy, $T = 26$ °C; and (b) effect of temperature (state of charge = 100%) for the $\text{LaNi}_{4.30}\text{Mn}_{0.70}$ alloy. The inset represent the data at the higher frequencies.

metal hydride alloys.^{25,29-32} According to this, the exchange current density (i_o) for this reaction was evaluated from the radius (R_{ct}) of this arc, using the Butler-Volmer equation in the limit of low overpotentials, that is,

$$i_o = \frac{RT}{nF} \left(\frac{1}{R_{ct}} \right)_{\eta \rightarrow 0}$$

where, F is the Faraday's constant, R the gas constant, and T the temperature. Measurements of i_o were conducted at the open circuit potential (reversible potential) at several temperatures in order to obtain the activation energy (E^\ddagger) of the hydrogen oxidation step. Figure 7 illustrates the

Arrhenius plots of i_0 vs. $1/T$ from which the activation energies were obtained. In Figure 8 the values of E^\ddagger obtained at 26 °C, 100 % state of charge, are plotted as a function of the alloy maximum HSC.

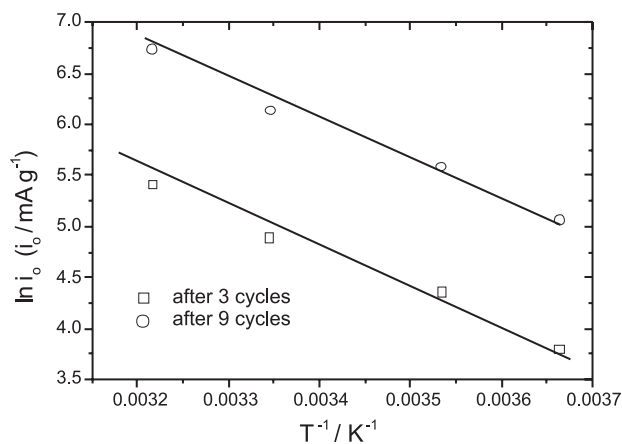


Figure 7. Arrhenius plots for the exchange current density for the electrode prepared with the $\text{LaNi}_{4.7}\text{Al}_{0.3}$ alloy, after different charge/discharge cycling steps.

Results in Figure 7 show a significative increase of i_0 with the increase of activation cycle number for the $\text{LaNi}_{4.7}\text{Al}_{0.3}$ alloy. However, results indicate that the activation energy has the same value in the both cases (29 kJ mol^{-1}). In this way, the increase of i_0 with the cycle number must be exclusively attributed to the increase of the active area resulting from the initially large stress cracking process.

From the results in Figure 8 it is observed that generally, the alloys with larger HSC are those presenting smaller E^\ddagger .

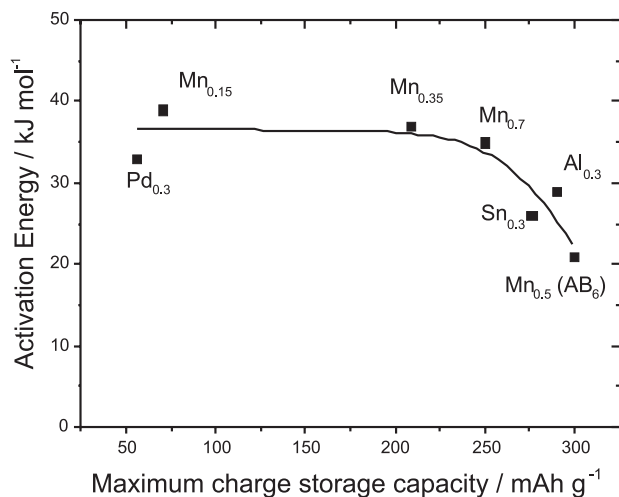


Figure 8. Activation energy at 26 °C, 100 % state of charge, as a function of the hydrogen storage capacity (HSC) for the different alloys.

This fact indicates that the same property that determines the charge storage capacity must also govern the kinetics of the electron transfer reaction. As mentioned before, this must be the occupancy of the Ni $3d$ band which is an important factor controlling the strength of the M-H bond. This last property is a crucial parameter for determining the magnitude of the activation energy barrier and the chemical potential of H in the hydride phase, and thus the kinetics of HOR and the magnitude of the HSC, respectively.

Table 3. Values of the activation energy E^\ddagger obtained for AB_5 and AB_6 alloys

Type	Composition	E^\ddagger (kJ mol^{-1})
AB_5	$\text{LaNi}_{4.7}\text{Sn}_{0.3}$	26
	$\text{LaNi}_{4.7}\text{Al}_{0.3}$	29
	$\text{LaNi}_{4.7}\text{Pd}_{0.3}$	35
	$\text{LaNi}_{4.85}\text{Mn}_{0.15}$	39
	$\text{LaNi}_{4.65}\text{Mn}_{0.35}$	37
	$\text{LaNi}_{4.30}\text{Mn}_{0.70}$	33
AB_6	$\text{LaNi}_{5.50}\text{Mn}_{0.50}$	21

Conclusions

Results indicate that specific electronic effects determine the cell volume characteristics for most of the metal hydride alloys. Substitution of a small fraction of Ni by Al, Sn, and Mn leads to an increase of the hydrogen storage capability of the metal hydride alloys, while for Pd the effect is the opposite. No correlations can be established between the HSC and the unit cell volumes, indicating that electronic effects of the substituents on the Ni band occupancy are more important than the changes in the cell volume to define the HSC. Generally, the alloys presenting larger initial HSC exhibit lower cycling stability. This indicates that a larger insertion of H in the unit cell leads to higher volume expansion, raising the stress-cracking and thus the corrosion rates.

A decrease of the hydrogen equilibrium pressure as a function of Mn content is observed and this is clearly related to an increase of the crystalline unit cell volume. There is a significant increase of the hydration/dehydration reaction kinetics due to a raise on the active area as a function of the charge/discharge cycle number. The alloys presenting larger HSC are those showing smaller activation energies for the hydrogen oxidation reaction. This must be due to different occupancy of the Ni $3d$ band which is an important fact controlling the strength of the M-H bond, and thus the kinetics of HOR and the magnitude of the HSC.

Acknowledgements

The authors thank the Fundação de Amparo à Pesquisa do Estado de São Paulo (FAPESP), Coordenação de Aperfeiçoamento de Pessoal de Nível Superior (CAPES), and Conselho de Desenvolvimento Científico e Tecnológico (CNPq), for financial supports.

References

1. Linden, D.; *Handbook of Batteries*, Mc Graw-Hill, Inc.: New York, 1995, p.1.
2. Ratnakumar, B.V.; Witham, C.; Bowman Jr., R.C.; Hightower, A.; Fultz, B.; *J. Electrochem. Soc.* **1996**, *143*, 2578.
3. Yu, J.; Lee, S.; Cho, K.; Lee, J.Y.; *J. Electrochem. Soc.* **2000**, *147*, 2013.
4. Guo, J.H.; Jiang, Z.T.; Duan, Q.S.; Liu, G.Z.; Zhang, J.H.; Xia, C.M.; Guo, S.Y.; *J. Alloys Comp.* **1999**, *293-295*, 821.
5. Kuriyama, N.; Sakai, T.; Miyamura, H.; Tanaka, H.; Uehara, I.; Meli, F.; Schlapbach, L.; *J. Alloys Comp.* **1996**, *238*, 128.
6. Adzic, G.D.; Johnson, J.R.; Reilly, J.J.; McBreen, J.; Mukerjee, S.; Kumar, M.P.S.; Zang, W.; Srinivasan, S.; *J. Electrochem. Soc.* **1995**, *142*, 3429.
7. Witham, C.; Ratnakumar, B.V.; Bowman Jr., R.C.; Hightower, A.; Fultz, B.; *J. Electrochem. Soc.* **1996**, *143*, L206.
8. Vogt, T.; Reilly, J.J.; Johnson, J.R.; Adzic, G.D.; McBreen, J.; *J. Electrochem. Solid-State Lett.* **1999**, *2*, 111.
9. Notten, P.H.; Latroche, M.; Percheron-Guégan, A.; *J. Electrochem. Soc.* **1999**, *146*, 3181.
10. Feng, F.; Han, J.; Geng, M.; Northwood, D.O.; *Solar Energy Materials Solar Cells* **2000**, *62*, 51.
11. Liang, G.; Huot, J.; Schultz, R.; *J. Alloys Comp.* **2001**, *320*, 133.
12. Adzic, G.D.; Johnson, J.R.; Mukerjee, S.; McBreen, J.; Reilly, J.J.; *J. Alloys Comp.* **1997**, *253-254*, 579.
13. Vogt, T.; Reilly, J.J.; Johnson, J.R.; Adzic, G.D.; McBreen, J.; *J. Electrochem. Soc.* **1999**, *146*, 15.
14. Züttel, A.; Gross, K.; Schlapbach, L.; *J. Alloys Comp.* **1996**, *241*, 160.
15. Xue, Q.; Xueping, G.; Jiansheng, C.; Huatang, Y.; Deying, S.; *Proceedings of the 13th World Hydrogen Energy Conference*, Beijing, China, June 2000.
16. Lu, H.; Gao, X.P.; Song, D.Y.; Zhang, Y.S.; *J. Alloys Comp.* **1996**, *238*, 110.
17. Matthew, L.A.; Anderson, I.E.; *J. Alloys Comp.* **2000**, *313*, 47.
18. Yan, D-Y.; Suda, S.; *J. Alloys Comp.* **1995**, *223*, 28.
19. Bowman, R.C.; Witham, C.; Fultz, B.; Ratnakumar, B.V.; Ellis, T.W.; Anderson, I.E.; *J. Alloys Comp.* **1997**, *253-254*, 613.
20. Feng, F.; Geng, M.; Northwood, D.O.; *J. Hydrogen Energy* **2001**, *26*, 727.
21. Reilly, J.J.; Adzic, G.D.; Johnson, J.R.; Vogt, T.; Mukerjee, S.; McBreen, J.; *J. Alloys Comp.* **1999**, *293-295*, 569.
22. Geng, M.; Feng, F.; Sebastian, P.J.; Matchett, A.J.; Northwood, D.O.; *Proceedings of the 13th World Hydrogen Energy Conference*, Beijing, China, June 2000.
23. *International Tables for X-Ray Crystallography*, D. Riedel Publishing Company: Dordrecht, 1985, vol. 4, p. 279.
24. Geng, M.; Han, J.; Feng, F.; Derek, O.; Northwood, D.O.; *J. Electrochem. Soc.* **1999**, *146*, 1650.
25. Ticianelli, E.A.; Mukerjee, S.; McBreen, J.; Adzic, G.D.; Johnson, J.R.; Reilly, J.J.; *J. Electrochem. Soc.* **1999**, *146*, 3582.
26. Mukerjee, S.; McBreen, J.; Reilly, J.J.; Johnson, J.R.; Adzic, G.D.; Petrov, K.; Kumar, M.P.S.; Zang, W.; Srinivasan, S.; *J. Electrochem. Soc.* **1995**, *142*, 2278.
27. Ploehn, H.J.; White, R.E.; *J. Electrochem. Soc.* **1998**, *145*, 1840.
28. Züttel, A.; Meli, F.; Schlapbach, L.J.; *J. Alloys Comp.* **1995**, *221*, 207.
29. Yang, H.; Zhang, Y.; Zhou, Z.; Wei, J.; Wang, G.; Song, D.; Cao, X.; Wang, C.; *J. Alloys Comp.* **1995**, *231*, 625.
30. Senoh, H.; Ueda, M.; Furukuwa, N.; Inoue, H.; Iwakura, C.; *J. Alloys Comp.* **1998**, *280*, 114.
31. Zhang, W.; Kumar, M.P.S.; Srinivasan, S.; Ploehn, H.J.; *J. Electrochem. Soc.* **1995**, *142*, 2936.
32. Wang, C.; *J. Electrochem. Soc.* **1998**, *145*, 1801.

Received: January 10, 2003

Published on the web: August 8, 2003

FAPESP helped in meeting the publication costs of this article.